Impedance analysis of eddy current fields on inhomogeneous conductive medium with stress corrosion cracks

Institute of Fluid Science, Tohoku University
Taishi Okita, Toshiyuki Takagi and Tetsuya Uchimoto
2-1-1 Katahira, Aoba-ku, Sendai, 980-8577, Japan
okita@wert.ifs.tohoku.ac.jp

We numerically compute the impedance of the probe-coil as an eddy-current signal due to stress corrosion cracks (SCC) and/or fatigue cracks in the conductive and nonmagnetic materials by using 3D finite element model. The fine shallow cracks with various structures are self-consistently simulated by providing zero-conductivity with a part of the background materials. We find the significant difference in the coil impedance, which crucially depends on the crack geometries. Our model and the obtained results would be helpful in understanding the eddy-current behavior around the cracks, and also in predicting the internal crack structures

Keywords: Eddy-Current, Finite Element Method, Stress Corrosion Crack, Fatigue Crack

1. Introduction

The eddy-current nondestructive evaluation (NDE) has commonly been used in order to detect the surface breaking defects such as SCC and fatigue cracks in the critical metal structures of i.e., aerospace, power generation, and manufacturing industries [1-4]. When the skin depth of the induced electromagnetic fields is comparable to the characteristic scale of the defects, the surface defect on the material may give an important effect on the eddy-current flow, which induces the secondary return magnetic fields, and hence generates the change in the impedance of the detection coil. In the NDE technique, the eddy-current is excited by the probe coil carrying an alternating electric current in the frequency range of 1 kHz - 10 MHz. In such a low frequency regime, one can generally adopt the quasistatic approximation, in which the displacement current of Ampare-Maxwell's equations can safely be neglected [5].

Flaw detection will become optimum when the skin depth of the fields is smaller than the characteristic scale of the flaw. This limit is often referred to as a thin skin regime. Analytical calculations of the coil impedance have so far widely been studied in explicit geometries by many authors by calculating the induced electromagnetic fields inside and outside the homogeneous conductive test-piece in the thin skin limit, in which the boundary conditions are applied on the crack mouth in such a way that the total magnetic flux is conserved [6,7].

The signal from the SCC in the conductive materials will significantly be different from that of fatigue cracks, since the geometrical internal structure of the SCC is quite complicated compared to the fatigue cracks.

The final objective of this work is to investigate the effect of the crack geometry, magnetism, and the inhomogeneity of the materials on the coil impedance. We numerically calculate the induced electromagnetic field distributions in the conductive materials with a surface defect with various structures. Calculations will be performed in a finite element method by exploiting the simulation package for the electromagnetic field analysis developed by PHOTON Co., Ltd [8]. Real and imaginary parts of the coil impedance are computed for some representative crack geometries.

2. Basic equations

In the quasistatic limit, where the effects of the induced charge density and the permittivity are ignored, the governing equation for the vector potential $\vec{A}$ of the magnetic fields can be dissolved into two explicit forms. In this work, all physical quantities of the fields are assumed to vary harmonically in time with a frequency ω. In a free space, outside the conductor, the formula results in the well-known Poisson equation

$$\nabla^2 \vec{A}_0 = \mu_0 \vec{J}_0, \qquad (1)$$

where μ_0 is a magnetic permeability in the vacuum, $\vec{J}_0$

is an electric current density of the driving coil. In the conductor with a magnetic permeability μ and an electric conductivity σ, the solution can be found by solving the Helmholtz equation

$$\nabla^2 \vec{A} - i\omega\mu\sigma\vec{A} = 0. \quad (2)$$

Equations (1) and (2) should be solved subject to the boundary conditions for the vector potential on the surface of the conductor and/or the crack plane

$$\vec{n} \times \vec{A}_0 = \vec{n} \times \vec{A}, \quad (3)$$

$$\frac{1}{\mu_0} \vec{n} \times \nabla \times \vec{A}_0 = \frac{1}{\mu} \vec{n} \times \nabla \times \vec{A}, \quad (4)$$

$$\vec{A} \cdot \vec{n} = 0, \quad (5)$$

$$\nabla \cdot \vec{A}_0 = 0, \quad (6)$$

where $\vec{n}$ is a unit vector normal to the conductive surface. Once the vector potential is given, the electromotive force (EMF) V of the probe-coil can readily be obtained by calculating

$$V = \omega \oint_C \mathrm{Im}\left[\vec{A}\right] \cdot d\vec{s} - i\omega \oint_C \mathrm{Re}\left[\vec{A}\right] \cdot d\vec{s}, \quad (7)$$

where ds is an infinitesimal length along the current path.

3. Finite element model

The finite element model for analyzing the electromagnetic fields is shown in Fig.1. The conductive test piece has a dimension of 20 mm x 20 mm x 5 mm. The driving and the detection coils of 1 turn with the inner radius 1 mm and the thickness 0.1 mm are lifted-off 0.1 mm above the surface of the test piece, whose conductivity is assumed to be 10^6 Sm^{-1} throughout the paper. The source coil is supplied by the alternating electric current with the amplitude 1 A and the excitation frequency 10 kHz. The skin depth can thus be estimated to be 1.6 mm for the nonmagnetic conductor. The effect of the eddy-current in the coil are not important and are neglected in the calculation for simplicity. The coil impedance in the absence of the defect can straightforwardly be calculated by infilling the crack with the mother materials.

In this work, four kinds of typical structures of the SCC are simulated, as shown in Fig.2. From the top, thick rectangle shaped crack, thin rectangle crack, a pair of parallel cracks, and branched crack. Every crack has the same length 2 mm and the same depth 2 mm, which are larger than the skin depth. The cracks are located at the center of the test piece. The EMFs are calculated for the four crack structures, when scanning the probe-coil at 10 intervals with the scan distance 30 mm in the crack direction (x-direction).

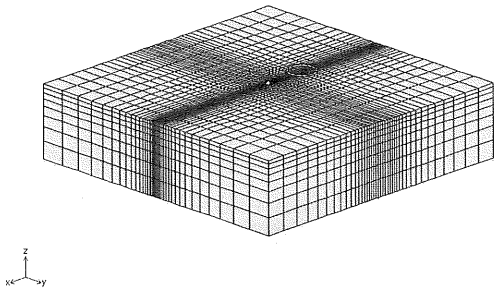

Fig. 1. The finite element model for calculating the induced electromagnetic fields inside and outside the conductive test piece with a uniform conductivity 10^6 Sm^{-1}.

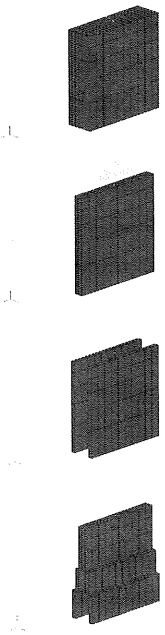

Fig. 2. Four representative geometries of the cracks with zero-conductivities, which are embedded in the test piece shown in Fig.1.

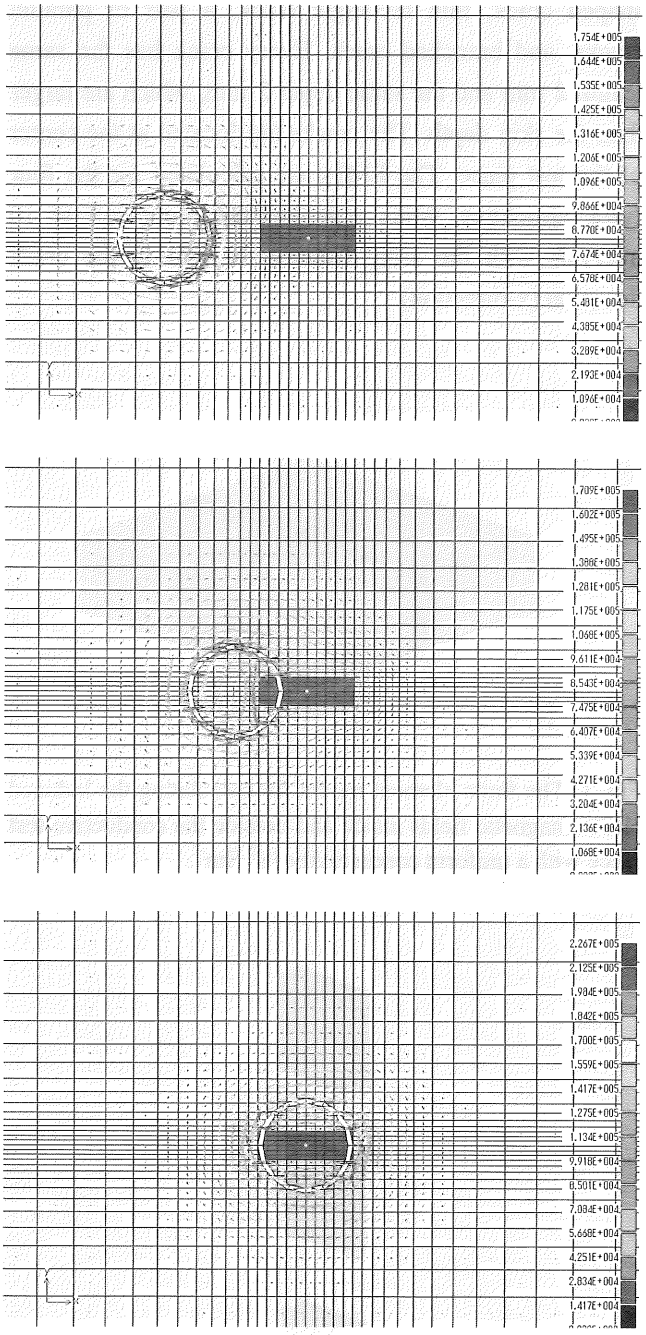

Fig. 3. Eddy-current distributions on the surface layer of the conductor with the thick-rectangular crack at some coil locations.

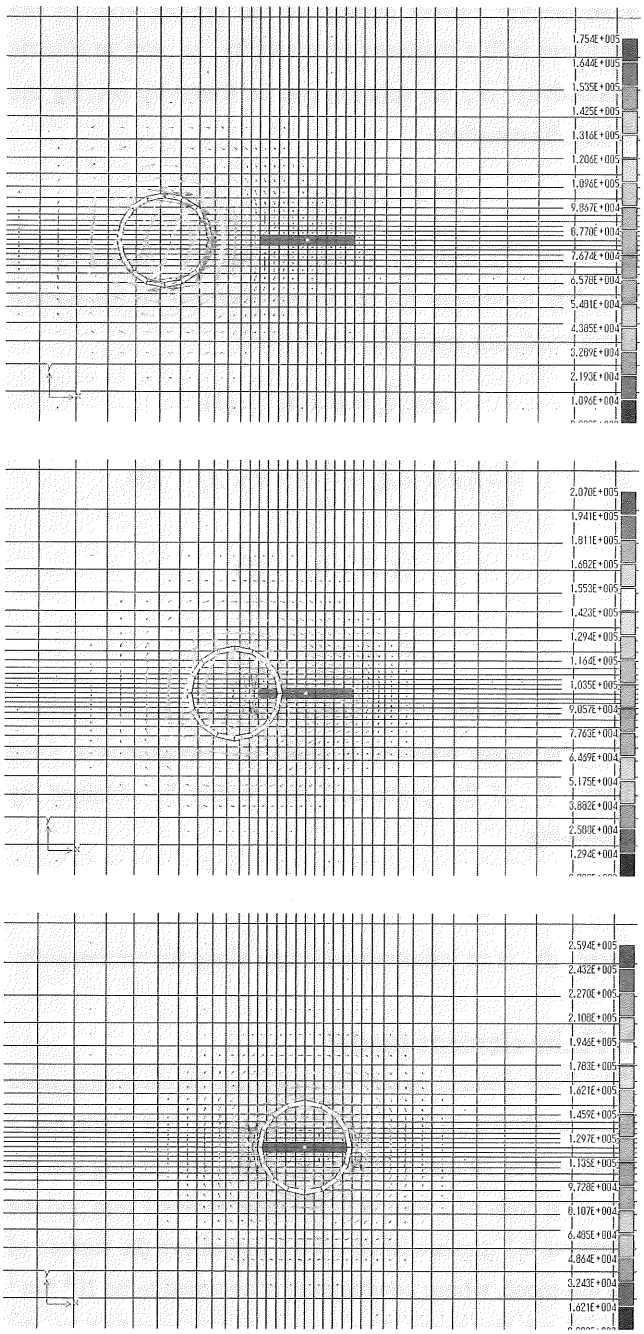

Fig. 4. Eddy-current distributions on the surface layer of the conductor with the thin-rectangular crack at some coil locations.

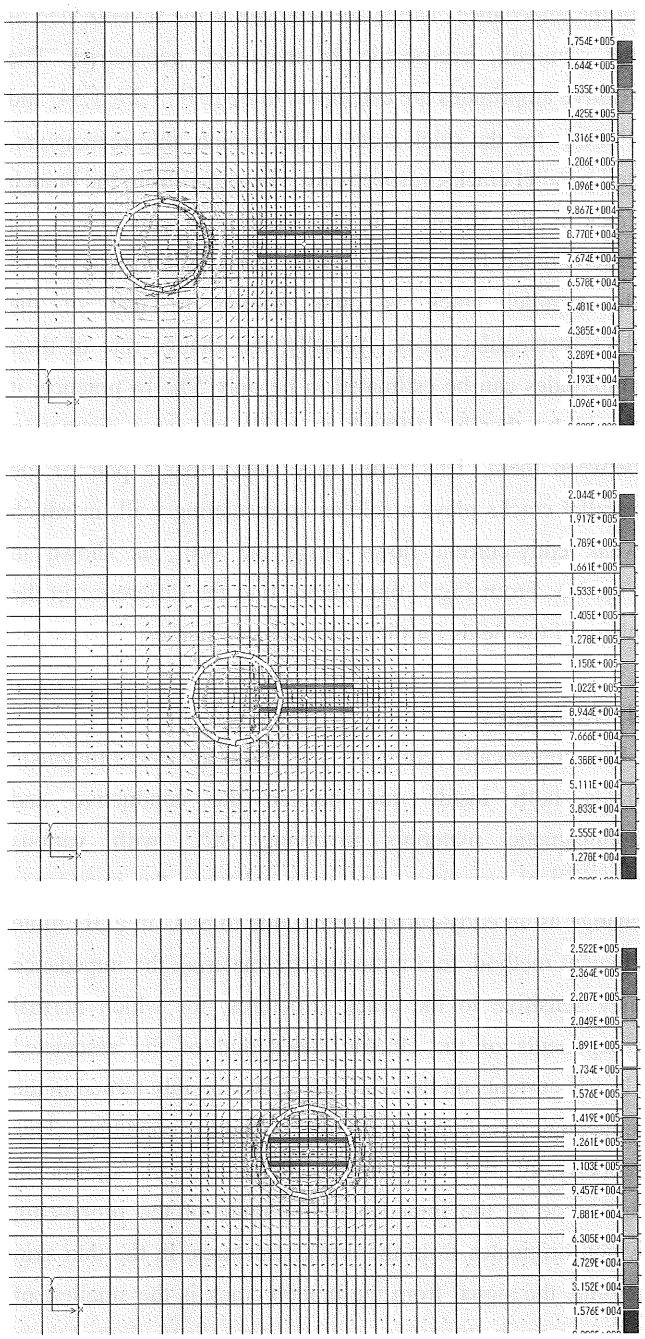

Fig. 5. Eddy-current distributions on the surface layer of the conductor with a pair of the parallel cracks at some coil locations.

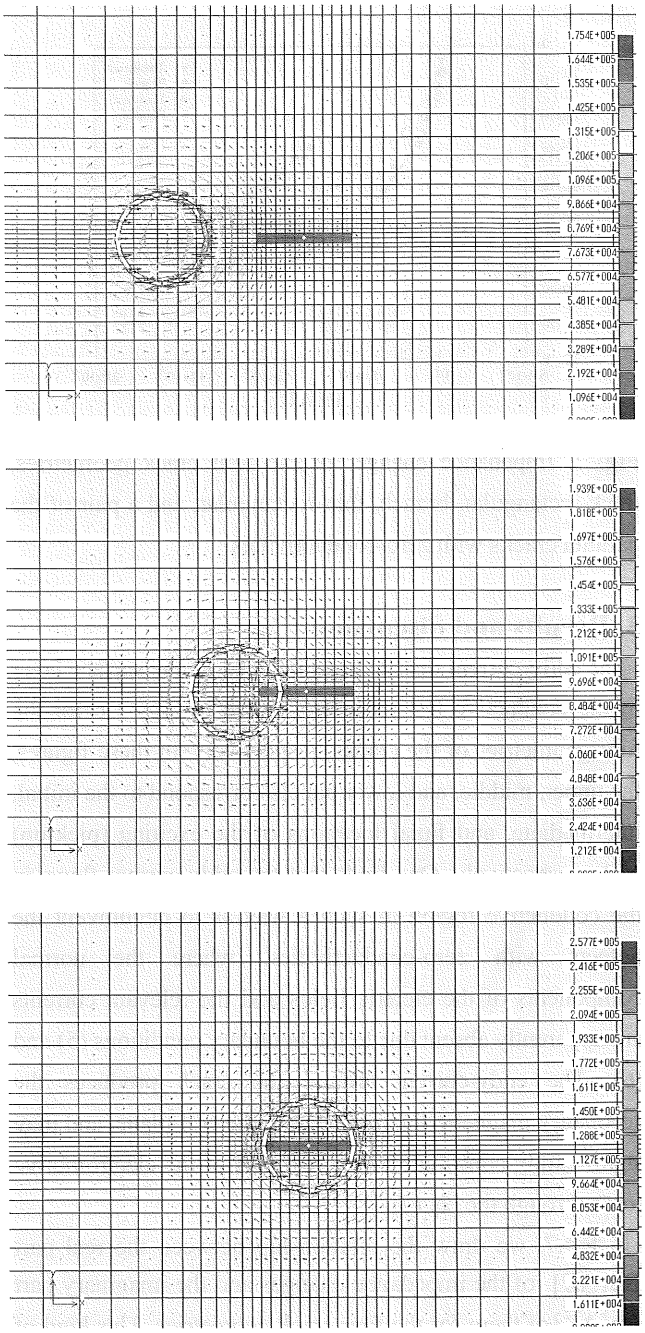

Fig. 6. Eddy-current distributions on the surface layer of the conductor with the branch cracks at some coil locations.

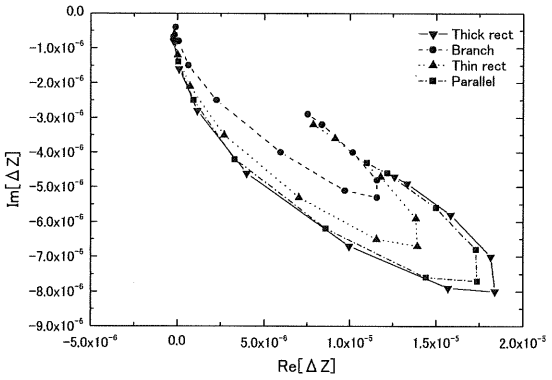

Fig. 7. Impedance change for the four crack geometries, thick-rectangular, branch, thin-rectangular, and a pair of the parallel cracks with zero-conductivities.

3. Results and discussion

The eddy-current distributions induced on the surface layer of the conductive test piece are shown in Figs 3-6 for the four geometries of the cracks, respectively. In these figures, the upper, middle, and lower panels correspond to the initial, intermediate, and finial locations of the exciting (pick-up) coils, respectively. One finds that the eddy-current flows in the conductive region in such a way as to circumvent the defects with zero-conductivities, where the normal components of the electric fields and the relevant currents are apparently absent due to the boundary conditions (5) and (6). The eddy-current around the crack produces the secondary magnetic flux permeating the coil-plane, and may significantly contribute to the real part of the electromotive force through the eq. (7).

In Fig.7, we draw the relationship between the real part $\mathrm{Re}[\Delta Z]$ of the impedance changes and the imaginary part $\mathrm{Im}[\Delta Z]$ of them for the four crack geometries. This kind of curves are often referred to as *Lissajou* diagram. In the thin skin regime, the real part of the impedance will be associated with the surface resistive effect for the fields at the crack mouth and/or the edge. While the imaginary part may be due to the electromagnetic energy stored in the crack volume [9,10]. We now define the relative amplitudes A of the impedance change as

$$A = |\Delta Z| = \sqrt{(\mathrm{Re}[\Delta Z])^2 + (\mathrm{Im}[\Delta Z])^2}, \qquad (8)$$

The *Lissajou* diagram shows that the maximum amplitudes of the impedance change are achieved at the seventh step of the scan-coil, irrespective of the crack geometries. The relative amplitudes are calculated to be 2.01, 1.27, 1.54, and $1.90\,\Omega$ for the thick-rectangular, branch, thin-rectangular, and parallel cracks, respectively. The signal from the branch crack is the smallest in our model. It can clearly be differentiated from other signals. The *Lissajou* behavior of the parallel crack is quite similar to that of the thick-rectangular crack. Actually, the change rate of their amplitudes can be estimated to be only 5%. In practice, it would be thereby difficult to make an exact distinction between them. This result may imply that a pair of the parallel cracks plays a role as an insulating wall, in which weak eddy-current flows along the wall, as shown in Figs.3-6. From Fig.7, one cannot find the difference in the phase of the fields for the four crack geometries.

4. Summary

We numerically compute the induced electromagnetic fields both inside and outside the conductive and nonmagnetic materials involving SCC with various geometrical structures, and then calculate the impedance change as an eddy-current signal due to SCC in a 3D finite element method. In a nonmagnetic material, the impedance may sensitive to the crack structures, for which normal components of the electric fields and of the associated electric currents on the crack plane are forcibly turned in the tangential direction due to the boundary condition. This property of the eddy-current fields induces significant difference in the impedance amplitude of the probe-coil, which originates from the crack structures. In the thin-skin regime, the signal from the branch crack is the smallest of the four crack structures, and is clearly discriminated from other signals, if the characteristic scales of the defects are almost same. However, the difference in the phase cannot be found in our model.

In this preliminary work, we have assumed that the conductive test piece and the nonconductive cracks are homogeneous, nonmagnetic and also linear. Specifically, the magnetic property of the medium, even if small, may give rise to the drastic change of the impedance of the coil [11]. The effect of the magnetism of the materials on the impedance will be investigated in the future work.

Aknowledgment

We are greatly obliged to Dr. T. Abe for technical suggestions with regards metal materials.

References

[1] R. C. McMaster, P. M. McIntyre, and M. L. Mester, *Nondestructive Testing Handbook*, 2nd ed., **4** (American Society for Nondestructive Testing, Philadelphia) (1986)

[2] Z. Badics, et al., *Journal of Nondestructive Evaluation*, **14**, 181 (1995)

[3] P. C. French and L. J. Bond, *Journal of Nondestructive Evaluation*, **7**, 55 (1988)

[4] J. D. Jackson, *Classical Electrodynamics*, John Wiley & Sons, New York (1975)

[5] T. P. Theodoulidis and J. R. Bowler, *Journal of Applied Physics,* **103**, 024905 (2008)

[6] A. M. Lewis, *Journal of Physics D*: *Applied Physics*, **25**, 319 (1992)

[7] S. K. Burke, *Journal of Applied Physics*, **76**, 3072 (1994)

[8] http://www.photon-cae.co.jp/

[9] A. H. Kahn, R. Spal, and A. Feldman, *Journal of Applied Physics,* **48**, 4454 (1977)

[10] N. Harfield and J. R. Bowler, *Journal of Applied Physics,* **82**, 4590 (1997)

[11] E. Uzal, J. C. Moulder, S. Mitra, and J. H. Rose, *Journal of Applied Physics,* **74**, 2076 (1993)